Journal of Biomedical Optics

SPIEDigitalLibrary.org/jbo

Acoustic and photoacoustic characterization of micron-sized perfluorocarbon emulsions

Eric M. Strohm
Ivan Gorelikov
Naomi Matsuura
Michael C. Kolios

SPIE

Acoustic and photoacoustic characterization of micron-sized perfluorocarbon emulsions

Eric M. Strohm,[a] Ivan Gorelikov,[b] Naomi Matsuura,[b] and Michael C. Kolios[a]
[a]Ryerson University, Department of Physics, Toronto, Canada
[b]Sunnybrook Health Sciences Centre, Imaging Research Department, Toronto, Canada

Abstract. Perfluorocarbon droplets containing nanoparticles (NPs) have recently been investigated as theranostic and dual-mode contrast agents. These droplets can be vaporized via laser irradiation or used as photoacoustic contrast agents below the vaporization threshold. This study investigates the photoacoustic mechanism of NP-loaded droplets using photoacoustic frequencies between 100 and 1000 MHz, where distinct spectral features are observed that are related to the droplet composition. The measured photoacoustic spectrum from NP-loaded perfluorocarbon droplets was compared to a theoretical model that assumes a homogenous liquid. Good agreement in the location of the spectral features was observed, which suggests the NPs act primarily as optical absorbers to induce thermal expansion of the droplet as a single homogenous object. The NP size and composition do not affect the photoacoustic spectrum; therefore, the photoacoustic signal can be maximized by optimizing the NP optical absorbing properties. To confirm the theoretical parameters in the model, photoacoustic, ultrasonic, and optical methods were used to estimate the droplet diameter. Photoacoustic and ultrasonic methods agreed to within 1.4%, while the optical measurement was 8.5% higher; this difference decreased with increasing droplet size. The small discrepancy may be attributed to the difficulty in observing the small droplets through the partially translucent phantom. [DOI: 10.1117/1.JBO.17.9.096016]

Keywords: perfluorocarbon droplets; contrast agent; nanoparticles; acoustic microscopy; photoacoustic imaging; dispersion.

Paper 12243P received Apr. 19, 2012; revised manuscript received Jul. 30, 2012; accepted for publication Aug. 21, 2012; published online Sep. 18, 2012.

1 Introduction

For several decades, perfluorocarbon (PFC) liquids have been used in various biomedical applications. PFCs are biologically and chemically inert, which makes them appealing for use in medicine,[1] and they can be emulsified into nano- or micron-sized droplets[2] to overcome their insolubility in water for *in vivo* infusion. In 2000, it was reported that a liquid-to-gas phase change could be induced in PFC emulsions via ultrasound irradiation using a method called acoustic droplet vaporization (ADV).[3,4] The resulting bubbles could be used as ultrasound contrast agents,[4–7] for cancer therapy via vessel occlusion,[8] and enhance thermal ablation with high-intensity focused ultrasound (HIFU).[9] Furthermore, upon vaporization, chemotherapeutic agents loaded within the emulsions can be released to deliver drugs to a target region.[10,11] Recently, PFC emulsions have been developed as photoacoustic agents through the incorporation of optically absorbing nanoparticles (NPs)[12–15] or dyes[16] into the droplets. NP-loaded PFC droplets can be vaporized via light using a method called optical droplet vaporization (ODV)[13,14] with similar applications as in ADV. Alternatively, the droplets could be irradiated below their vaporization threshold where they remain as liquid particles and used as photoacoustic contrast agents.[14,15]

NPs in the 10 to 200 nm range have been used as photoacoustic contrast agents *in vivo*,[17–19] where they circulate within the bloodstream and extravasate into tumors via the enhanced permeability and retention effect (EPR).[20] Using PFC droplets containing NPs as photoacoustic contrast agents may provide advantages over using NPs alone. The NPs within a droplet are concentrated into a small volume, so fewer NPs may be required to create a measurable photoacoustic signal compared to free NPs. The photoacoustic signal from NPs is dependent on the environment surrounding the NP.[21] Enclosing the NPs within a droplet of known liquid allows for direct optimization of the NPs within the liquid to maximize the photoacoustic signal output, whereas the signal from free NPs may differ depending on their location (such as blood, interstitial tissue, or within single cells). It is also possible to functionalize the PFC droplet surface with targeting ligands or imaging agents.[22] These droplets can be loaded with therapeutic agents to deliver a targeted payload to a region of interest.[10,11] Finally, the droplet size can be tailored for specific applications, ranging from nm-sized (for penetration into interstitial tissue) to micron-sized (restricted to the bloodstream). The droplets could be used as photoacoustic contrast agents to determine their location and then vaporized to release a payload and/or the NPs into surrounding tissue. There have been very few studies examining the photoacoustic mechanism from NP-loaded droplets.

NPs are increasingly being used as photoacoustic contrast agents. This paper demonstrates that micron-sized PFH droplets loaded with optical absorbing, silica-coated gold NPs act as a single photoacoustic emitter when irradiated with the appropriate wavelengths and can be used as photoacoustic contrast agents. The droplet photoacoustic spectral features, from droplets of various sizes, are investigated to show that the droplet photoacoustic spectrum features depend on the size and physical properties of the liquid within the droplet only. The NPs are only

Address all correspondence to: Michael C. Kolios, Ryerson University, Department of Physics, Toronto, Canada. Tel: +416-979-5000 x7065; E-mail: mkolios@ryerson.ca

0091-3286/2012/$25.00 © 2012 SPIE

used to initiate the thermal expansion within the droplet. These findings indicate the NP-loaded droplets provide advantages over using NPs alone.

2 Theory

When irradiated by a laser with an appropriate wavelength, optically absorbing structures will absorb energy and undergo a rapid thermoelastic expansion, resulting in emission of a pressure wave that can be detected with conventional ultrasonic transducers. In this study, silica-coated gold NPs were selected as the optical absorbers, due to their strong absorption peak at the laser frequency used, and their ability to be loaded within the PFC droplets.[14] A well-established theoretical model was used to calculate the photoacoustic pressure waves generated from homogeneous optical absorbing liquid spheres.[23] Assuming the droplet undergoes a uniform thermal expansion due to the heated NPs, the frequency domain pressure wave generated a distance r from a droplet with radius a when irradiated with a laser intensity I_0 is

$$P(f) = i\left(\frac{\mu_a I_0 c_d \beta}{4\pi C_p (r/a)}\right) \times \frac{(\sin q - q\cos q)/q^2}{\left(1-\frac{\rho_d}{\rho_f}\right)(\sin q/q) - \cos q + i\frac{c_d}{c_f}\frac{\rho_d}{\rho_f}\sin q}, \quad (1)$$

where f is the ultrasound frequency, β is the droplet thermal expansion coefficient, C_p is the droplet heat capacity, μ_a is the optical absorption coefficient of the NPs within the droplet, ρ is the density, c is the sound speed, the subscripts d and f refer to the droplet and surrounding fluid, respectively, and $q = 2\pi f a/c_d$.[23] In this equation, the variables in the first bracket contribute only to the amplitude of the signal and can be represented by a constant A. The only variables that contribute significantly to spectral variations [the component to the right of the bracket in Eq. (1)] are the droplet radius, density, and sound speed. This equation also assumes that the physical parameters such as sound speed do not change with frequency. Although this assumption is valid for liquids where sound dispersion is absent over small frequency ranges, in this study a frequency range of 100 to 1000 MHz was used, where PFC liquids have a small but measureable increase in sound speed with frequency.[24] To account for this dispersion, Eq. (1) was modified by setting the droplet sound speed as a function of frequency, and setting the variables that contribute to the amplitude to a constant A, so that the pressure P as a function of frequency is

$$P(f) = iA\frac{(\sin q - q\cos q)/q^2}{\left(1-\frac{\rho_d}{\rho_f}\right)(\sin q/q) - \cos q + i\frac{c_d(f)}{c_f}\frac{\rho_d}{\rho_f}\sin q}, \quad \text{where } q = \frac{2\pi f a}{c_d(f)}. \quad (2)$$

The droplet radius, density, and sound speed all contribute to the frequency content of the generated photoacoustic signal. If the PFC liquid type [e.g., perfluorohexane (PFH)] is kept constant, then the droplet radius is the only parameter that affects the photoacoustic spectral features. The droplet diameter can be calculated by adjusting the radius in the model until a best fit between the model and measured photoacoustic spectrum is found. To confirm the accuracy of the diameter parameter in the model, the diameter can also be determined using photoacoustic and ultrasonic pulse echo methods based on the time of flight of the photoacoustic signals or reflected echoes from the droplet surfaces. A characteristic "N-shape" wave in the time domain is generated composed of a positive pressure followed by a negative pressure.[25] If the sound speed c_d in the droplet is known, the droplet diameter can be found from the arrival time of the pressures wave using

$$d = c_d(t_2 - t_1), \quad (3)$$

where t_1 is time of flight of the positive pressure peak and t_2 is the time of flight of negative pressure peak. Similarly, when a droplet is probed with pulsed ultrasound, echoes will occur from the top and bottom of the droplet due to the acoustic impedance mismatch between the droplet and surrounding fluid. The diameter of the droplet can be found using

$$d = \frac{c_d}{2}(t_2 - t_1), \quad (4)$$

where t_1 is the echo from the top of the droplet and t_2 is the echo from the bottom of the droplet.[26] In total, four independent methods were used to determine the PFC droplet diameters in this study.

In Eq. (2), it is essential to know how the sound speed varies as a function of frequency (known as sound dispersion). Previous work measuring the sound speed and attenuation of PFC liquids determined that the sound speed and ultrasound attenuation of PFH increases with frequency.[24] The increase in attenuation $\alpha(f)$ with frequency is generally described using a power law fit, such as $\alpha(f) = \alpha_0 f^n$, where the attenuation coefficient α_0 and the power law exponent n describe how the attenuation changes with frequency.[27] A direct relationship between sound dispersion and ultrasonic attenuation can be accurately described using the Kramers-Kronig relation[28]

$$c(f) = \left[\frac{1}{c_d} + \alpha_0 \tan\left(\frac{n\pi}{2}\right)(|2\pi f|^{n-1} - |2\pi f_0|^{n-1})\right]^{-1}, \quad (5)$$

where $\alpha_0 = \alpha(f)/f^n$ is the attenuation coefficient (with units Nepers, converted to dB by multiplying by 8.686), and f_0 is the frequency where c_d was measured.[29] The change in sound speed with frequency can be determined using equation 5 if α_0 and n are known for a specific liquid.

3 Method

3.1 *PFC Emulsions*

Gold NPs were synthesized using a previously published method based on the reduction of sodium citrate.[30] Specifically, gold NPs were made by loading 100 mg of sodium citrate and 150 mL of deionized water into a 250-mL round-bottom flask, heating the mixture to boiling, followed by the injection of 1 mL of 25 mM $HAuCl_4$. The temperature of the mixture was slowly decreased to 90°C over a 15 min time period, and 1 mL of 60-mM sodium citrate was then injected, followed by the injection of 0.9 mL of 25-mM $HAuCl_4$. After 15 min, the injections of sodium citrate and $HAuCl_4$ were repeated, resulting in the formation of gold NPs. To miscibilize gold NPs into PFHs (FC-72, Synquest Labs, FL, USA), the NPs were coated with silica,[31] followed by surface fluorination.[32,33] Specifically, to coat the NPs with silica, a freshly prepared aqueous solution of 3-aminopropyl trimethoxy silane (APTES, 1.6 mL, 1 mM) was

added to 150 mL of the gold NPs solution under vigorous magnetic stirring. The APS and gold dispersion were reacted for 15 min to ensure complete complexation of the amine groups with the gold surface. A solution of active silica was prepared by lowering the pH of a 0.54 wt% sodium silicate solution to 11 by progressive additions of 1.0 M HCl. Active silica (9 mL) was then added to 150 mL of the surface modified gold NPs, again under vigorous magnetic stirring. The resulting dispersion (pH = 8.5) was then allowed to stand for a minimum of 24 h, to permit the active silica to polymerize onto the surface of the gold NPs. For miscibilization of gold NPs into PFH, the silica-coated gold NPs were redispersed in 10 mL of methanol,[34] and the mixture was reacted with 150 μL of 1H,1H,2H,2H-perfluorodecyltriethoxysilane (5 min), and mixed with 50 μL of 30% ammonia/water and reacted for 24 h. After evaporation of methanol, the NPs were solubilized into 2 mL of PFH. All chemicals for silica-coated gold NP synthesis and their miscibilization into PFCs ($HAuCl_4$, sodium citrate, APS, sodium silicate and 1H,1H,2H,2H-perfluorodecyltriehthoxysilane) were purchased from Sigma-Aldrich, ON, Canada. The thickness of the silica coating and the size of the gold NPs were determined by transmission electron microscopy using a Hitachi S-5200 scanning electron microscope (Hitachi Canada Ltd., ON, Canada). For NP characterization in the ultraviolet, visible, and near-IR ranges, a Cary-5000 UV-Vis-NIR spectrophotometer (Agilent Technologies, CA, USA) was used. Gold NP-incorporated PFH droplets were prepared using 5 mL of deionized water (Millipore Milli-Q grade, 18.2 MΩ), 0.175 mL of gold NP-FC-72 solution, and 0.025 mL of anionic phosphate fluorosurfactant (Zonyl-FSP, Sigma Aldrich, ON, Canada). Droplets were prepared by coarse emulsification by vortexing, followed by membrane emulsification using 10-μm pore size polycarbonate membranes (Nuclepore Track-Etch Membrane, Whatman, NJ, USA).[14]

PFH (56°C boiling point) was used instead of the more commonly used perfluoropentane (PFP, 29°C boiling point) as micron-scale PFH droplets are more stable and are less likely to spontaneously vaporize at the temperatures used in these experiments compared to PFP droplets.[35,36] Moreover, the sound speed of bulk PFP could not be measured at 36°C as it is over the boiling point of 29°C, and it would be difficult to use the theoretical photoacoustic equations. The sound speed of bulk PFH has been previously measured at the frequencies and temperatures used.[24]

3.2 *Photoacoustic Microscope*

All acoustic and photoacoustic measurements were made using the SASAM acoustic microscope (Kibero GmbH, Germany). An IX81 inverted optical microscope (Olympus, Japan) was modified where a transducer was positioned above the optical objective. The sample is positioned between the optical objective and transducer, allowing for optical observation during measurements. Ultrasonic pulse echo measurements were made by scanning the sample under the transducer. For photoacoustic measurements, a 532-nm laser was collimated through the back port of the inverted microscope and focused onto the sample with the same objective used to view the sample. A dichoric mirror (Chroma Technology Corp, USA) was used to reflect optical wavelengths between 450 and 620 nm, but pass all other wavelengths to allow for optical viewing and targeting when using the laser [Fig. 1(a)]. The transducer was focused above the laser spot under optical guidance, and the sample

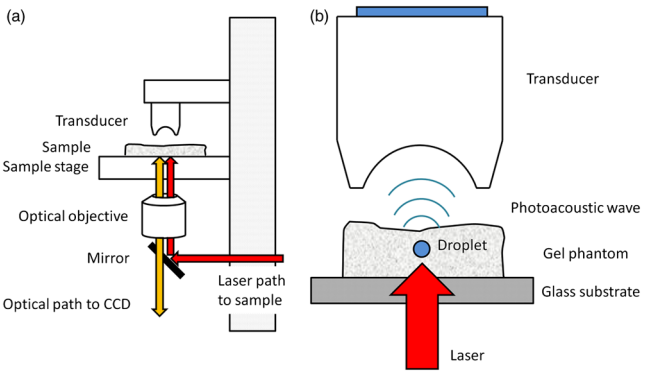

Fig. 1 (a) The acoustic microscope is an inverted optical microscope where the laser has been focused through the pack port onto the sample. The mirror reflects 500 to 650 nm (the laser wavelengths) toward the sample, but allows other wavelengths to pass for optical viewing. The transducer measures the signals from above the sample. (b) A close-up view of a measurement of a single droplet. The laser is focused onto the sample using the optical objective with the transducer positioned directly above the droplet.

was scanned under the transducer with both the optical objective and transducer remaining stationary [Fig. 1(b)].

Transducers with center frequencies of 375 MHz (60-deg aperture, 42% bandwidth) and 750 MHz (100-deg aperture, 37% bandwidth) were used for all acoustic and photoacoustic measurements. For acoustic measurements, a 10 V_{pp} monocycle signal was generated at 300 MHz (for the 375 MHz transducer) and at 1000 MHz (for the 750 MHz transducer) at a pulse repetition frequency (PRF) of up to 500 kHz. One hundred signals were averaged at 375 MHz, while 1000 signals were averaged at 750 MHz. For photoacoustic measurements, the laser was focused onto the sample using a 10× optical objective (0.3 numerical aperture). The laser triggered the data acquisition of the signals the transducer recorded. The laser had a pulse width of 330 ps and PRF of 4 kHz. All signals were amplified by a 40-dB amplifier (Miteq, USA) and digitized at 8 GHz. All measurements were made at 36°C to simulate human physiological conditions. Further details on the system can be found elsewhere.[14,37]

3.3 *Acoustic and Photoacoustic Measurements*

Droplets were embedded into gelatin phantoms to ensure they were immobilized during the measurements. Droplets were added to liquid gelatin at a temperature of 37°C, and then formaldehyde was added to increase phantom stiffness. Droplets close to the phantom surface were measured to minimize the attenuation losses through gelatin. All acoustic and photoacoustic measurements at 375 MHz were made with the droplets embedded within the gelatin. No signal from embedded droplets was detected at 750 MHz due to attenuation through the gelatin, therefore droplets were deposited onto the phantom surface for the 750-MHz photoacoustic measurements. Subsequent measurements using the 375-MHz transducer were not possible, as the droplets would move from the field of view while switching transducers. The acoustic properties of gelatin and water are very similar,[38] and the spectral features only depend on the sound speed and density of the droplet and coupling fluid in Eq. (2). Therefore it is unlikely the change in medium between similar liquids would significantly affect the spectral shape.

To record the acoustic and photoacoustic signals, a droplet was positioned over the laser spot and then the transducer was focused above the droplet. The sample stage was scanned over a 10×10-μm area using a 0.5-μm step size, and the signal from the center of the droplet was used for analysis. The optical objective and transducer remained stationary and co-aligned during all scans. The transducer response was removed by normalizing the signal as described elsewhere.[39] Briefly, the normalized signal was calculated by dividing the measured spectrum of the droplet by the reference spectrum of the transducer. The bandwidth of a transducer is typically found by measuring the reflected echoes from a glass or quartz substrate that reflects the ultrasound back to the transducer. We have found that this is not an accurate representation of the transducer bandwidth used in photoacoustics since the transducer is used in passive mode. The transducers appear to have better sensitivity when receiving (photoacoustic) than during transmit and receive (ultrasound). A 200-nm gold layer theoretically has a flat photoacoustic spectrum to within 3 dB from 1 to 1000 MHz,[40] and will give an accurate representation of the transducer spectral response in passive mode; therefore, we used the photoacoustic signal from a gold film as a reference. A Hamming window was applied to all signals, along with a bandpass filter of 100 to 500 MHz for the 375-MHz transducer and 300 to 1000 MHz for the 750-MHz transducer.

3.4 *Droplet Diameter Measurements*

The droplet diameter was calculated using three independent methods: 1) the photoacoustic time domain signal; 2) the time domain ultrasound signal; and 3) fitting the measured photoacoustic spectrum to the model. Only the signals measured using the 375-MHz transducer were used in the diameter calculations. These calculations were compared to images recorded from a CCD camera using an optical microscope with a 10× objective ($100 \times$ total magnification).

The photoacoustic method used the time of flight of the positive and negative pressure waves from the droplet and Eq. (3) to determine the droplet diameter. The pressure wave emitted from a droplet during optical irradiation has two significant features: an initial positive sharp pressure peak that gradually decreases to a negative pressure peak. This waveform has a characteristic "*N*-shape" in the time domain, analogous to pressure waves generated from a bursting balloon.[41,42] The theoretical time domain signal for a 5-μm PFH droplet is shown in Fig. 2(a) (black dotted line), where the *N*-shape waveform is clearly visible. However, the finite bandwidth of a transducer can alter the signal. For example, the same signal subjected to a Hamming window and a 100- to 500-MHz bandpass filter (to emulate the limited transducer bandwidth) is shown in Fig. 2(a) (red solid line). Instead of an N-shape, two peaks are visible, which align with the positive and negative peaks of the *N*-shape waveform. These two peaks can be used to determine the droplet diameter using Eq. (3), where t_1 is the positive peak on the first signal and t_2 is the negative peak on the second signal.

The ultrasound pulse echo method used the time of flight of the echoes from the top and bottom of the droplet [t_1 and t_2 in Fig. 2(b)] in Eq. (4) to determine the droplet diameter. This approach required that the droplet was sufficiently large so that the two echoes were separated in time and could be resolved. This method could not be used for droplets smaller than approximately 5 μm, as the signals would overlap.

The photoacoustic spectral method was used to calculate the diameter by comparing the spectrum from the measured photoacoustic signal to the model [Eq. (2)]. The model was calculated using a constant density of 1650 kg/m^3, and the sound speed was varied from 480 to 486 m/s with increasing frequency from 100 to 1000 MHz [Eq. (5)]. The diameter was adjusted until the minima and maxima between experiment and model matched. The diameter found from these signal processing methods were then compared to a direct optical measurement from the microscope.

4 Results and Discussion

4.1 *Droplet Configuration*

Silica-coated gold NPs were used as the optical absorbing NP in this study due to their strong optical absorption peak around 540 nm. Transmission electron microscopy images demonstrated these NPs were of uniform size, with a 20-nm-diameter core and 5-nm-thick silica shell [Fig. 3(a)]. The optical absorption of the PFH solution containing NPs peaked between 530 to 540 nm [Fig. 3(b)], an optimum range for the 532-nm pulsed laser used in this study. The laser energy for all photoacoustic measurements was 30 nJ/pulse, focused to a spot size approximately 10 μm in diameter, resulting in a laser fluence of 38 mJ/cm^2. Although damage to gold NPs has been reported for laser fluences as low as 25 mJ/cm^2 at 532 nm,[43] damage

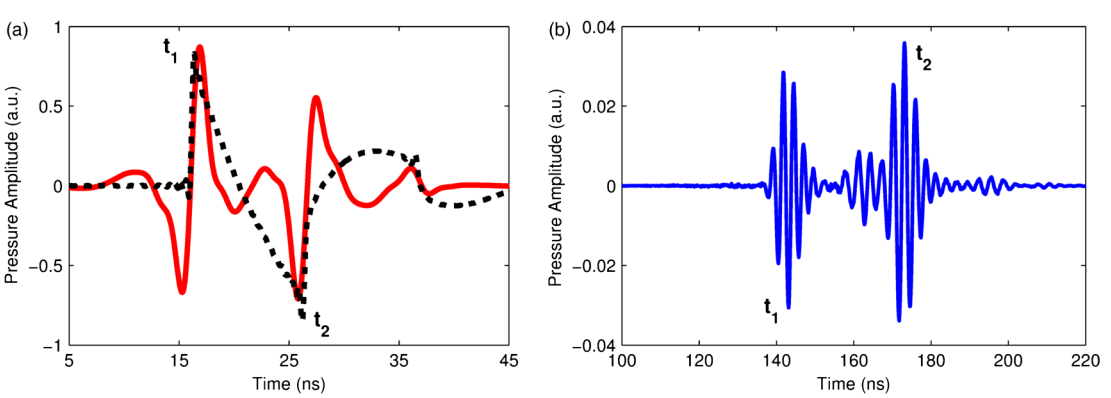

Fig. 2 (a) The theoretical photoacoustic time domain signal from a 5-μm droplet using Eq. (2) (black dotted line), and the same signal after applying a Hamming window and 100- to 500-MHz bandpass filter (red solid line). (b) The measured ultrasound echoes from a 7.2-μm PFH droplet embedded in gelatin. The signals labeled t_1 and t_2 were used to determine the droplet diameter using Eq. (3) (photoacoustic, left) and Eq. (4) (ultrasound, right).

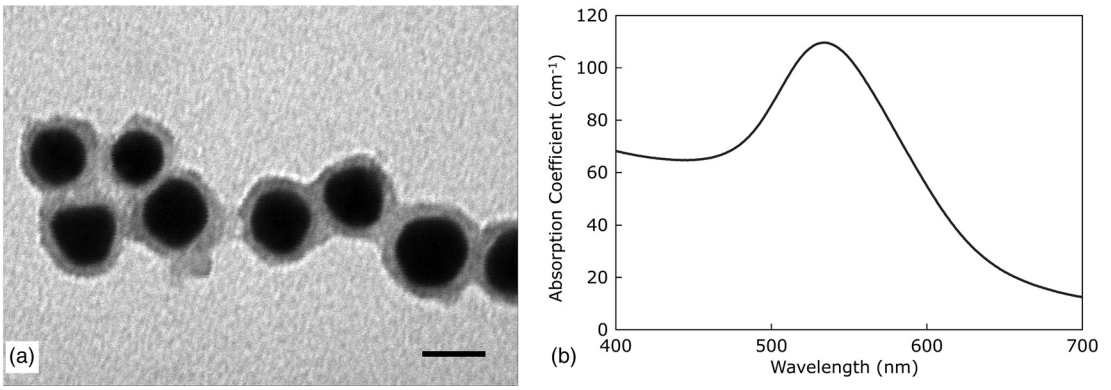

Fig. 3 Transmission electron microscopy image (a) and optical absorption coefficient (b) of the silica coated gold NP PFH solution. The gold NPs were approximately 20 nm in diameter with a 5 nm thick silica coating. The peak optical absorption was between 530 and 540 nm. The scale bar is 20 nm.

thresholds can depend on the gold NP surface and coating, and other laser parameters such as pulse length. In this study, the photoacoustic signals from the NP-loaded droplets (ranging in size from 2 to 15 μm) were stable over repeated measurements using laser fluences of 38 mJ/cm^2, indicating damage to NPs was negligible. At higher fluence levels (over 50 mJ/cm^2), the measured photoacoustic signal decreased rapidly over repeated pulses, which could be attributed to NP damage. The vaporization threshold for these droplets was between 50 and 120 mJ/cm^2, considerably less than 1.5 to 3 J/cm^2 required to vaporize PFH droplets containing lead sulphide NPs reported previously using a 1064-nm laser.[14] This is likely due to the much higher absorption coefficient of the gold NPs (110 cm^{-1} at 532 nm) compared with lead sulphide NPs (4.3 cm^{-1} at 1064 nm).

The number of NPs inside the droplets was estimated based on the initial concentration of NPs in the PFC liquid ($\sim 10^{14}$ NPs/mL of PFC). Assuming the NPs are distributed uniformly within the droplets, there are approximately 6550 NPs in 5-μm droplets (6.7×10^{-11} cc) and 52300 NPs in 10-μm droplets (5.7×10^{-10} cc). The approximate distance from one NP to its neighbor can be calculated by estimating the volume fraction of spheres that can fill a single droplet using a random close-packing model.[44] Based on this model, the average distance between NPs is ~230 nm. Although some nonuniform distribution of NPs within the droplets is possible, as an order of magnitude calculation, the calculated values for the NP quantity and NP-spacing seem reasonable.

4.2 *Sound Dispersion Effects*

Other studies have demonstrated excellent agreement between the photoacoustic model [Eq. (1)] and experiments of optical absorbing mm-sized spherical droplets at photoacoustic frequencies less than 20 MHz, where sound dispersion has been neglected.[23,25,45] While PFC liquids have negligible dispersion at 22 MHz,[46] a small but measureable increase of sound dispersion was found for three PFC liquids up to 1000 MHz.[24] For PFH, the liquid used in this study, the sound speed increased from 480 to 486 m/s, and the ultrasound attenuation increased from 1368 to 16840 dB/cm from 200 to 1000 MHz at 36°C.[24] Using a power law fit, the attenuation as a function of frequency was found to be $\alpha(f) = 0.352\ f^{1.56}$, as described in Ref. 24. Attenuation is linked to changes in sound speed via the Kramers-Kronig relations. To obtain a smooth change in sound speed with frequency, the sound speed over the range of 100 to 1000 MHz was calculated from the attenuation power law fit of $0.352\ f^{1.56}$ using the Kramers-Kronig relations [Eq. (5)].

The effects of this small but measurable amount of dispersion is shown in Fig. 4, which compares the theoretical time and frequency domain solution using Eq. (1) (constant sound speed) with Eq. (2) (increasing sound speed) for a 5-μm diameter

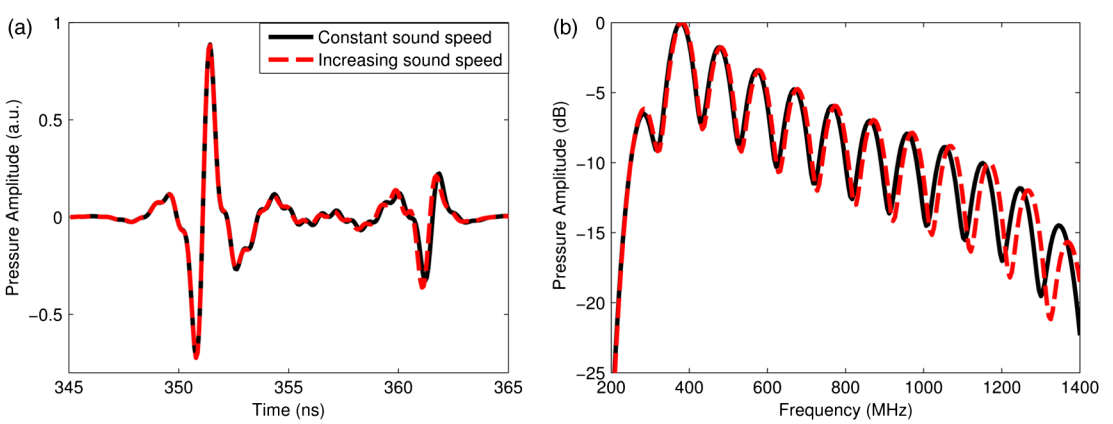

Fig. 4 The effects of dispersion on the photoacoustic model showing the time domain solution (a) and frequency domain solution (b) for a 5-μm droplet using Eq. (1) (constant sound speed, black solid line) and Eq. (2) (sound speed increasing from 480 to 486 m/s, red dashed line). A Hamming window and 300- to 1400-MHz bandpass filter were used for both solutions. Good agreement was found up to 300 MHz, but discrepancies in the location of the spectral minima and maxima were observed over 500 MHz.

PFH droplet. A Hamming window and 300- to 1400-MHz bandpass filter were used to simulate a wide bandwidth transducer. Good agreement in the location of the spectral minima and maxima between both equations were observed up to 300 MHz, while discrepancies were observed over 500 MHz. Only minor differences were observed in the time domain waveform, where the second peak at 362 ns was shifted slightly. Since this study compares the measured photoacoustic spectra from droplets up to 1000 MHz, it is important to account for sound dispersion when comparing measured results to the model.

4.3 *Droplet Diameter Measurements*

The diameters of 18 micron-sized droplets were calculated using the three signal-based methods (photoacoustic waveform, ultrasound pulse echo, and photoacoustic spectrum) and compared with optical microscopy measurements. The results are summarized in Table 1. The diameter was calculated using several methods to verify the photoacoustic spectral fit; in Eqs. (1) and (2), the spectral minima and maxima shift depending on q, which itself depends on the droplet radius and sound speed. The same photoacoustic spectrum could be obtained by varying the droplet radius and sound speed, provided the ratio remained constant. Therefore to ensure the parameters found from the spectral fit were accurate, they were compared to other methods.

The average difference in diameter between the three signal-based methods was 0.12 ± 0.09 μm. The direct optical measurement was an average 0.68 ± 0.39 μm greater than the other three methods. While the three calculated methods based on signal measurement were very close to each other, the optical measurements were 8.5% higher. The droplet images recorded were only 10 to 20 pixels across, which significantly reduced the measurement precision. Poor contrast due to difficulties in observing the droplet through the gelatin phantom prevented higher magnification objectives from being used. Due to the number of pixels used and the difficulty in observing the droplet through the phantom, the uncertainty in the droplet diameters estimated from optical methods was determined to be ± 0.5 μm. The larger diameter estimation and uncertainty in the optical method is likely due to the difficulty in determining the edges of a small spherical object near the limits of optical resolution, compounded by the difficulty in seeing through the partially translucent gelatin phantom. The agreement between optical and signal processing methods improved as the droplet diameter increased; for example, the optical method was $13\% \pm 8\%$ greater for diameters 5 to 7 μm and was only $4.8\% \pm 3.2\%$ for diameters over 10 μm. Therefore, it can be inferred that the diameter determined through optical microscopy would likely improve if larger diameters or higher magnifications were used. Since it was difficult to determine the droplet diameter visually, using the signal-based measurements were essential to corroborate the diameter as predicted by the model [Eq. (2)].

4.4 *Photoacoustic Spectral Measurements*

The model [Eq. (2)] calculates the photoacoustic pressure wave emitted from a spherical homogeneous liquid undergoing thermoelastic expansion due to absorption of optical energy. To determine if the measured photoacoustic spectra from NP-loaded PFH droplets were in agreement with the model, the photoacoustic signals for three droplets of different sizes were measured: a 5.7-μm droplet measured at 375 MHz, a 2.45-μm droplet measured at 750 MHz, and a 6.95-μm droplet measured at 750 MHz (Fig. 5). No photoacoustic signal was detected for unloaded PFH droplets. All signals were normalized to maximum amplitude, and the droplet diameter was determined by matching the measured photoacoustic spectral maxima and minima to the model [Eq. (2)]. The diameter found from the spectral fit agreed well with the time domain photoacoustic and ultrasound methods used to calculate the diameter (see Table 1).

The measured spectra agreed well with the model in both the time and frequency domains for all three droplets (Fig. 5). The gold NPs act exclusively as the optical absorbing material within the droplets, yet the photoacoustic pressure wave emitted is based entirely on the PFH liquid properties, and not of the gold NPs. This is consistent with previous photoacoustic measurements using lead sulphide NPs inside PFC droplets, which showed good agreement in the spectral features between the

Table 1 The diameters of 18 droplets calculated using the photoacoustic time domain signal [Eq. (3)], the ultrasound time domain signal [Eq. (4)], spectral comparison between model and experiment [Eq. (2)], and optical microscopy. The uncertainties in the photoacoustic and ultrasound methods were calculated based on the accuracy of determining the locations of the signal peaks in Fig. 1, and the model uncertainty from the diameter variations in fitting the experiment to theory. The optical method uncertainty was large due to the difficulty in determining the droplet edges, and the limited number of pixels used when acquiring the droplet image.

	Droplet diameter (μm)			
Droplet Number	Photoacoustic	Ultrasound	Spectral fit	Optical
1	5.14 ± 0.09	5.21 ± 0.05	5.0 ± 0.1	6.3 ± 0.5
2	5.38 ± 0.09	5.40 ± 0.05	5.3 ± 0.1	5.7 ± 0.5
3	5.42 ± 0.09	5.62 ± 0.05	5.4 ± 0.1	6.9 ± 0.5
4	5.04 ± 0.09	5.16 ± 0.05	5.4 ± 0.1	5.7 ± 0.5
5	6.00 ± 0.09	5.66 ± 0.05	6.0 ± 0.1	6.9 ± 0.5
6	6.14 ± 0.09	6.22 ± 0.05	6.1 ± 0.1	6.3 ± 0.5
7	6.43 ± 0.09	6.46 ± 0.05	6.4 ± 0.1	7.4 ± 0.5
8	6.86 ± 0.09	6.98 ± 0.05	6.9 ± 0.1	7.4 ± 0.5
9	7.10 ± 0.09	7.20 ± 0.05	7.0 ± 0.1	7.4 ± 0.5
10	7.10 ± 0.09	7.06 ± 0.05	7.2 ± 0.1	8.0 ± 0.5
11	7.44 ± 0.09	7.51 ± 0.05	7.3 ± 0.1	8.0 ± 0.5
12	8.11 ± 0.09	8.21 ± 0.05	8.1 ± 0.1	9.1 ± 0.5
13	7.97 ± 0.09	8.06 ± 0.05	8.1 ± 0.1	8.6 ± 0.5
14	10.3 ± 0.1	10.56 ± 0.06	10.3 ± 0.1	10.9 ± 0.5
15	10.7 ± 0.1	10.82 ± 0.06	10.7 ± 0.1	10.9 ± 0.5
16	13.1 ± 0.1	13.25 ± 0.07	13.1 ± 0.1	14.3 ± 0.5
17	13.2 ± 0.1	13.37 ± 0.07	13.3 ± 0.1	14.3 ± 0.5
18	13.4 ± 0.1	13.56 ± 0.07	13.3 ± 0.1	13.7 ± 0.5

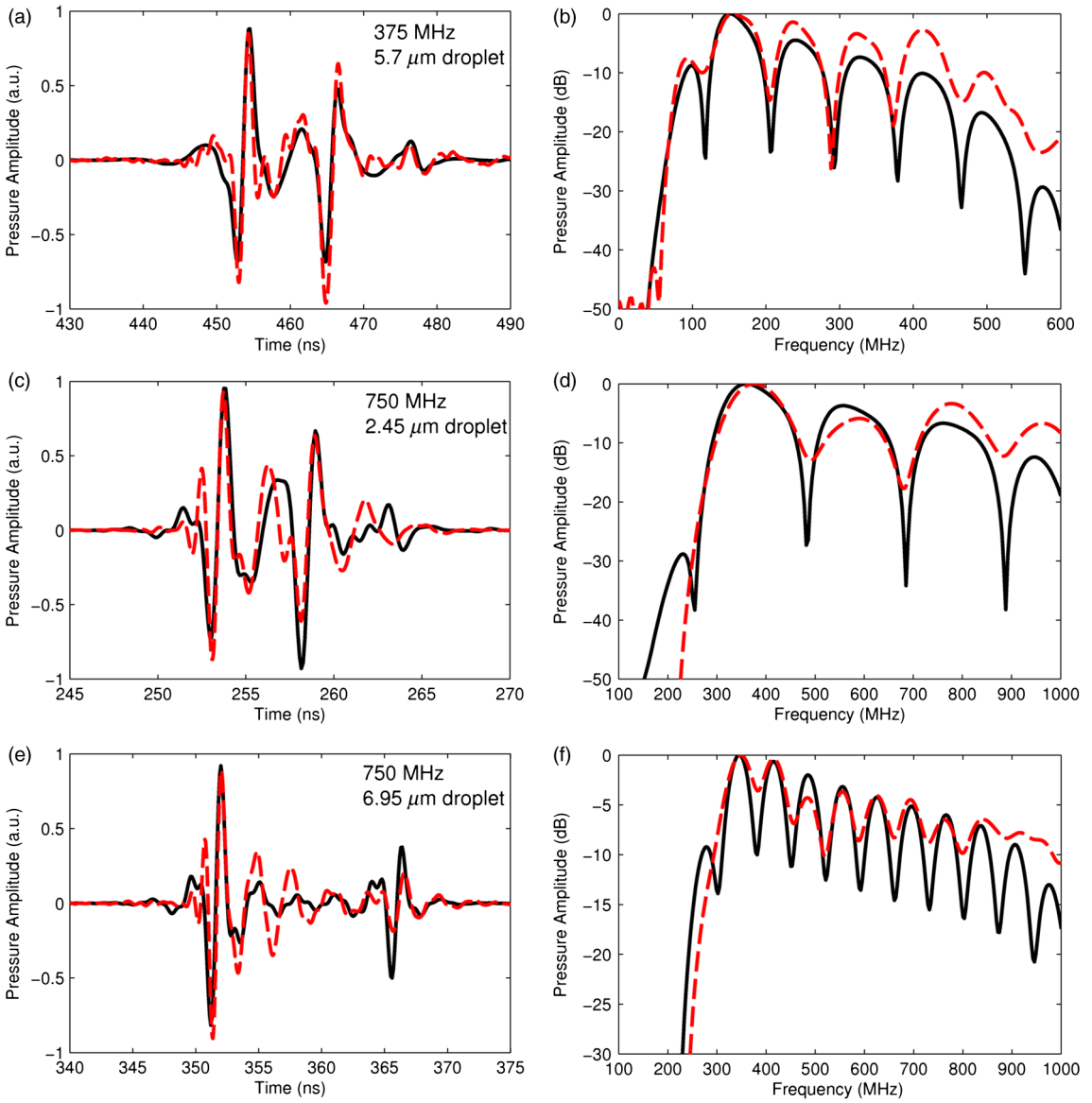

Fig. 5 The measured photoacoustic signal (red dashed line) compared to the model (black solid line, equation 2) for a 5.7-μm droplet measured at 375 MHz (a) and (b), a 2.45-μm droplet measured at 750 MHz (c) and (d) and a 6.95-μm droplet measured at 750 MHz (e) and (f). A bandpass filter of 100 to 500 MHz was used for the 375-MHz measurement, and a bandpass filter of 300 to 1000 MHz was used for the 750-MHz measurements. A Hamming window was applied to all measurements. Good agreement between model and experiment were found for the waveforms (a), (c), and (e), and in the location of the spectral minima and maxima (b), (d), and (f).

model and experiment.[47,48] These results also agree with a study that found the photoacoustic wave is generated from the liquid surrounding the NP, and not from the NP itself.[21] This suggests that the NP-loaded droplets can be modeled as a single photoacoustic source taking into account only the liquid PFC properties, irrespective of the optical absorbing NPs contained within, provided they absorb light sufficiently at the wavelength used. As NP-loaded emulsions gain popularity as photoacoustic contrast agents, the photoacoustic signal from droplets can be maximized by optimizing the size, shape, and type of NPs knowing that the emulsions will emit pressure waves as a single photoacoustic source.

5 Conclusions

The photoacoustic spectra of micron-sized NP-loaded PFH droplets measured from 100 to 1000 MHz were in good agreement to a theoretical model that calculates the pressure wave emitted from an optical absorbing droplet. Due to the fact that good agreement between experiment and theory was achieved using only the PFH liquid physical properties in the model, we conclude that the droplets behave as a single photoacoustic source based on the liquid properties such as the sound speed, density, and diameter and without regard to the NP composition. The NPs and liquids used in emulsions can be chosen to maximize optical absorption, knowing that the size and composition of the optical absorbing NPs have a negligible effect on the photoacoustic spectrum. In addition, four independent methods were used to determine the droplet diameter and corroborate the diameter determined from the photoacoustic spectral calculation. The three methods based on the photoacoustic and ultrasound signal processing methods agreed to within an average of 0.12 ± 0.09 μm, while the direct optical microscopy

measurement was 0.68 ± 0.39 μm higher. The large errors associated with the optical measurement may be due to limited visibility, poor contrast, and the difficulty in delineating the borders of micron-sized objects when embedded in a translucent gelatin medium.

Acknowledgments

E. Strohm is supported through a NSERC doctoral scholarship. This research was undertaken, in part, thanks to funding from NSERC and the Canada Research Chairs Program awarded to M. Kolios. Funding to purchase the equipment was provided by the Canada Foundation for Innovation, the Ontario Ministry of Research and Innovation, and Ryerson University. This study was supported, in part, by the Ontario Institute for Cancer Research Network through funding provided by the Province of Ontario, the FY07 Department of Defense Breast Cancer Research Program Concept Award (BC075873), a program project grant entitled "Imaging for Cancer" and "Ultrasound for Cancer Therapy" from the Terry Fox Foundation, and the Ontario Research Fund-Research for Excellence Program.

References

1. C. S. Cohn and M. M. Cushing, "Oxygen therapeutics: perfluorocarbons and blood substitute safety," *Crit. Care Clin.* **25**(2), 399–414 (2009).
2. J. P. Fast and S. Mecozzi, "Nanoemulsions for Intravenous Drug Delivery," in *Nanotechnology in Drug Delivery*, M. M. Villiers, P. Aramwit, and G. S. Kwon, Eds., 461–489, Springer New York, New York, NY (2009).
3. R. E. Apfel, "Activatable infusable dispersions containing drops of a superheated liquid," U. S. Patent No. 5840276 (1998).
4. O. D. Kripfgans et al., "Acoustic droplet vaporization for therapeutic and diagnostic applications," *Ultrasound Med. Biol.* **26**(7), 1177–1189 (2000).
5. T. Giesecke and K. Hynynen, "Ultrasound-mediated cavitation thresholds of liquid perfluorocarbon droplets in vitro," *Ultrasound Med. Biol.* **29**(9), 1359–1365 (2003).
6. P. S. Sheeran et al., "Decafluorobutane as a phase-change contrast agent for low-energy extravascular ultrasonic imaging," *Ultrasound Med. Biol.* **37**(9), 1518–1530 (2011).
7. N. Reznik, R. Williams, and P. N. Burns, "Investigation of vaporized submicron perfluorocarbon droplets as an ultrasound contrast agent," *Ultrasound Med. Biol.* **37**(8), 1271–1279 (2011).
8. O. D. Kripfgans et al., "In vivo droplet vaporization for occlusion therapy and phase aberration correction," *IEEE Trans. Ultrason. Ferroelectr. Freq. Control* **49**(6), 726–738 (2002).
9. M. Zhang et al., "Acoustic droplet vaporization for enhancement of thermal ablation by high intensity focused ultrasound," *Acad. Radiol.* **18**(9), 1123–1132 (2011).
10. M. L. Fabiilli et al., "Delivery of chlorambucil using an acoustically triggered perfluoropentane emulsion," *Ultrasound Med. Biol.* **36**(8), 1364–75 (2010).
11. N. Rapoport et al., "Ultrasound-mediated tumor imaging and nanotherapy using drug loaded, block copolymer stabilized perfluorocarbon nanoemulsions," *J. Control. Release* **153**(1), 4–15 (2011).
12. K. Wilson, K. Homan, and S. Emelianov, "Photoacoustic and ultrasound imaging contrast enhancement using a dual contrast agent," in *Proc. SPIE* **7564**, 75642P (2010).
13. E. M. Strohm et al., "Optical droplet vaporization (ODV): photoacoustic characterization of perfluorocarbon droplets," in *IEEE International Ultrasonics Symposium*, pp. 495–498, Institute of Electrical and Electronics Engineers (IEEE), USA (2010).
14. E. M. Strohm et al., "Vaporization of perfluorocarbon droplets using optical irradiation," *Bio. Opt. Express* **2**(6), 1432–1442 (2011).
15. K. Wilson, K. Homan, and S. Emelianov, "Biomedical photoacoustics beyond thermal expansion using triggered nanodroplet vaporization for contrast-enhanced imaging," *Nat. Commun.* **3**, 618 (Jan 2012).
16. W. J. Akers et al., "Noninvasive photoacoustic and fluorescence sentinel lymph node identification using dye-loaded perfluorocarbon nanoparticles," *ACS Nano* **5**(1), 173–182 (2011).
17. P. K. Jain, I. H. El-Sayed, and M. A. El-Sayed, "Au nanoparticles target cancer," *Nano Today* **2**(1), 18–29 (2007).
18. A. D. L. Zerda et al., "Carbon nanotubes as photoacoustic molecular imaging agents in living mice," *Nat. Nanotechnol.* **3**(9), 557–562 (2008).
19. J.-W. Kim et al., "Golden carbon nanotubes as multimodal photoacoustic and photothermal high-contrast molecular agents," *Nat. Nanotechnol.* **4**(10), 688–694 (2009).
20. H. Maeda et al., "Tumor vascular permeability and the EPR effect in macromolecular therapeutics: a review," *J. Control. Release* **65**(1–2), 271–284 (2000).
21. Y. Chen et al., "Environment-dependent generation of photoacoustic waves from plasmonic nanoparticles," *Small* **8**(1), 47–52 (2012).
22. M. M. Kaneda et al., "Perfluorocarbon nanoemulsions for quantitative molecular imaging and targeted therapeutics," *Ann. Biomed. Engin.* **37**(10), 1922–1933 (2009).
23. G. J. Diebold, T. Sun, and M. I. Khan, "Photoacoustic monopole radiation in one, two, and three dimensions," *Phys. Rev. Lett.* **67**(24), 3384–3387 (1991).
24. E. M. Strohm and M. C. Kolios, "Sound velocity and attenuation measurements of perfluorocarbon liquids using photoacoustic methods," in *IEEE International Ultrasonics Symposium*, pp. 2368–2371, Institute of Electrical and Electronics Engineers (IEEE), USA (2011).
25. G. J. Diebold, M. I. Khan, and S. M. Park, "Photoacoustic 'signatures' of particulate matter: optical production of acoustic monopole radiation," *Science* **250**(4977), 101–104 (1990).
26. A. Briggs and O. Kolosov, *Acoustic Microscopy*, Oxford University Press, USA (2009).
27. R. S. C. Cobbold, N. V. Sushilov, and A. C. Weathermon, "Transient propagation in media with classical or power-law loss," *J. Acoustical Soc. Am.* **116**(6), 3294–3303 (2004).
28. M. O'Donnell, "Kramers–Kronig relationship between ultrasonic attenuation and phase velocity," *J. Acoustical Soc. Am.* **69**(3), 696–701 (1981).
29. T. L. Szabo, "Causal theories and data for acoustic attenuation obeying a frequency power law," *J. Acoustical Soc. Am.* **97**(1), 14–24 (1995).
30. N. G. Bastús, J. Comenge, and V. Puntes, "Kinetically controlled seeded growth synthesis of citrate-stabilized gold nanoparticles of up to 200 nm: size focusing versus Ostwald ripening," *Langmuir* **27**(17), 11098–11105 (2011).
31. L. M. Liz-Marzán, M. Giersig, and P. Mulvaney, "Synthesis of nanosized gold–silica core–shell particles," *Langmuir* **12**(18), 4329–4335 (1996).
32. I. Gorelikov et al., "Silica-coated quantum dots for optical evaluation of perfluorocarbon droplet interactions with cells," *Langmuir* **27**(24), 15024–15033 (2011).
33. N. Matsuura et al., "Nanoparticle-tagged perfluorocarbon droplets for medical imaging," in *Mater. Res. Soc. Symp. Proc.* p. 1140, Cambridge University Press, Cambridge, United Kingdom (2009).
34. I. Gorelikov and N. Matsuura, "Single-step coating of mesoporous silica on cetyltrimethyl ammonium bromide-capped nanoparticles," *Nano Lett.* **8**(1), 369–373 (2008).
35. A. Martin et al., "Intracellular growth of nanoscale perfluorocarbon droplets for enhanced ultrasound-induced phase-change conversion," *Ultrasound Med. Biol.* **38**(10), 1799–1810 (2012).
36. M. G. Freire et al., "Aging mechanisms of perfluorocarbon emulsions using image analysis," *J. Colloid Interface Sci.* **286**(1), 224–232 (2005).
37. E. M. Strohm, G. J. Czarnota, and M. C. Kolios, "Quantitative measurements of apoptotic cell properties using acoustic microscopy," *IEEE Trans. Ultrason. Ferroelectr. Freq. Control* **57**(10), 2293–2304 (2010).
38. K. Zell et al., "Acoustical properties of selected tissue phantom materials for ultrasound imaging," *Phys. Med. Biol.* **52**(20), N475–N484 (2007).
39. R. E. Baddour et al., "High-frequency ultrasound scattering from microspheres and single cells," *J. Acoust. Soc. Am.* **117**(2), 934–943 (2005).
40. M. Khan, T. Sun, and G. Diebold, "Photoacoustic waves generated by absorption of laser radiation in optically thin layers," *J. Acoustical Soc. Am.* **93**(3), 1417–1425 (1993).
41. B. G. Watters, "The (sound of a bursting) red balloon," *Sound: Its Uses Control* **2**(2), 8–14 (1963).

42. D. T. Deihl, "'N Waves' from bursting balloons," *Am. J. Phys.* **36**(5), 441–444 (1968).
43. R. R. Letfullin et al., "Laser-induced explosion of gold nanoparticles: potential role for nanophotothermolysis of cancer," *Nanomedicine* **1**(4), 473–480 (2006).
44. G. D. Scott and D. M. Kilgour, "The density of random close packing of spheres," *J. Phys. D Appl. Phys.* **2**(6), 863–866 (1969).
45. G. Diebold and P. Westervelt, "The photoacoustic effect generated by a spherical droplet in a fluid," *J. Acoustical Soc. Am.* **84**, 2245–2251 (1988).
46. C. S. Hall et al., "Experimental determination of phase velocity of perfluorocarbons: applications to targeted contrast agents," *IEEE Trans. Ultrasonics Ferroelectr. Frequ. Control.* **47**(1), 75–84 (2000).
47. E. M. Strohm et al., "Optical droplet vaporization of micron-sized perfluorocarbon droplets and their photoacoustic detection," *Proc. SPIE* **7899**, 78993H (2011).
48. E. Strohm et al., "Photoacoustic spectral characterization of perfluorocarbon droplets," *Proc. SPIE* **8223**, 82232F (2012).